Mathematical Biosciences and Engineering

MBE, 20(3): 4896–4911.
DOI: 10.3934/mbe.2023227
Received: 28 November 2022
Revised: 21 December 2022
Accepted: 26 December 2022
Published: 04 January 2023

http://www.aimspress.com/journal/MBE

Research article

IDEFE algorithm: IDE algorithm optimizes the fuzzy entropy for the gland segmentation

Mingzhu Li[1], Ping Li[2] and Yao Liu[3,*]

[1] Department of Thyroid and Breast Surgery, East Branch of Quanzhou First Hospital, Fujian 362000, China
[2] Quanzhou First Hospital Affiliated to Fujian Medical University, Quanzhou, Fujian 362000, China
[3] College of Medicine, Huaqiao University, Quanzhou, Fujian 362021, China

* **Correspondence:** Email: yowk0529@gmail.com.

Abstract: Breast cancer occurs in the epithelial tissue of the gland, so the accuracy of gland segmentation is crucial to the physician's diagnosis. An innovative technique for breast mammography image gland segmentation is put forth in this paper. In the first step, the algorithm designed the gland segmentation evaluation function. Then a new mutation strategy is established, and the adaptive controlled variables are used to balance the ability of improved differential evolution (IDE) in terms of investigation and convergence. To evaluate its performance, The proposed method is validated on a number of benchmark breast images, including four types of glands from the Quanzhou First Hospital, Fujian, China. Furthermore, the proposed algorithm is been systematically compared to five state-of-the-art algorithms. From the average MSSIM and boxplot, the evidence suggests that the mutation strategy may be effective in searching the topography of the segmented gland problem. The experiment results demonstrated that the proposed method has the best gland segmentation results compared to other algorithms.

Keywords: gland segmentation; breast mammography; IDE algorithm; fuzzy entropy

1. Introduction

As reported by the Global Cancer Report [1], one in four women worldwide with new cancers is breast cancer, which is now the most prevalent cancer-related death in more than 100 countries. Breast

gland segmentation is one of the most important works in tumor detection. Breast image such as mammography, ultrasound, Magnetic Resonance (MR) and Computed Tomography (CT) are widely used in breast lesion detection [2]. Mammography images clearly show the layers of the breast and tiny calcifications and calcification clusters of less than 0.1 mm. The mammography inspection system has the characteristics of clear imaging, convenient, quick inspection operation, and small radiation [3]. Breast cancer development is significantly influenced by breast density and breast gland segmentation in digital mammogram is also reported for the purpose of diagnosis. In principle, Mammography images contain glandular area, which is critical for breast cancer prediction and tumor extraction. There have been many methods developed for image segmentation thus far [4,5].

These methods can be divided into four groups: region growing, pixel classification, threshold segmentation and model construction. The region expanding technique reduces merging between neighboring or overlapping structures by adjusting the original object boundaries using grayscale and gradient information, Petrick designed a segmentation of the breast mammary based on improved region growing techniques [6]. Otsu proposed a very popular image segmentation method to separate background and objects by maximizing the variance between classes based on Euclidean distance [7]. Tran and Wagner [8] proposed the fuzzy entropy clustering algorithm, and Bezdek et al. proposed the fuzzy C-means algorithm and the Snake model [9] can extract the target contours. Mario and Francesco [10] presented a new fuzzy edge detector based on both fuzzy divergence (thought and proved to be a distance) and fuzzy entropy minimization for the thresholding sub-step in gray-scale images. In their work, they test the proposed procedure after their fuzzification by a suitable adaptive S-shaped fuzzy membership function.

Building models for image segmentation is mainly based on convolutional neural networks (CNN). Mu et al. [11] proposed the PGPLP model, which is a computationally efficient full convolutional (FCN) network for COVID-19 CT image segmentation. However, it is difficult to detect small areas of infection in CT images with poor contrast. He et al. [12] developed a novel evolvable adversarial framework based on generating adversarial network (GAN) for COVID-19 infection segmentation. Experiments show that the method can improve the stability of segmentation, but focusing on the model hyperparameter adjustment appears to make the method complicated. Those method require enhancement and more intelligent AI architectures. However, typical deep learning is a fully deterministic model that is greatly influenced by the uncertainty of the data. Then, in addition to the points mentioned above, there is a huge limitation in the nature of the CNN approach, which is that when the image is input to the network at the initial stage, the model can only understand the input image using local information because the convolution kernel of the CNN is not too large, which inevitably has some blinders on, thus affecting the distinguishability of the features extracted by the encoder at the end. These are important reasons why we have not chosen to refer to CNN for our work.

A new method for gland segmentation of breast mammography images is proposed in this paper. Compared to previous work [11–16], our algorithm is chosen for gland segmentation because of two main advantages, 1) overcoming the two main limitations of optimization fuzzy entropy algorithms, which are the susceptibility to irregular edges and the premature convergence, and 2) faster convergence process and excellent solution. There are three aspects innovation for our proposed IDEFE algorithm. To address the premature convergence and slipping into local optimum entropy issues, the following technical contributions are proposed:

- the DE/current-to-K-best/1 is proposed in mutation operator, which can be achieved through the incorporation of best solution information in the evolutionary search;

- the parameter of adaptation F and CR are generated using Cauchy and normal distributions, with the goal of balancing global exploration and local exploitation during evolution;
- the application innovations use DE algorithms to optimize fitness, which can get the optimize threshold to segment breast glands.

Figure 1 shows the optimization of the evolutionary algorithm for glandular. As can be seen from Figure 1, the segmentation results become more and more accurate as the evolutionary algorithm is iterated. Therefore, the proposed method can solve the two main problems mentioned above at the same time. Experiments are conducted using 18 glandular mammography images from the Quanzhou First Hospital and the obtained results were compared with the recent swarm intelligent optimal segmentation method.

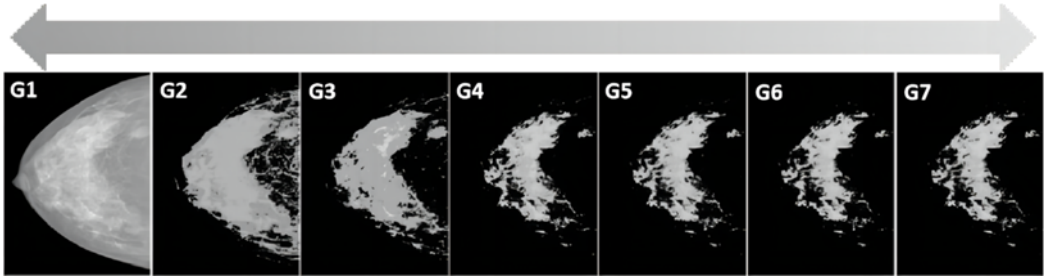

Figure 1. Evolutionary algorithm to optimize the segmentation process; G1: 0, G2: 5, G3: 10, G4: 20, G5: 30, G6: 50, G7: 100.

The remainder of this paper is structured as follows. The background information and related algorithms on which this work is based are presented in Section 2. Section 3 introduces the proposed method, an improved differential evolution based on fuzzy entropy (IDEFE) algorithm. Section 4 evaluates and compares the proposed method's performance to a set of algorithms from the literature. Finally, Section 5 brings the paper to a conclusion.

2. Related works

Fuzzy mathematical methods have a wide range of applications, including data mining [17,18], decision support and medical diagnosis, where the fuzzy principle can be applied to image processing. Since images usually exhibit uncertainty and noise interference problems, traditional segmentation methods often fail to achieve ideal segmentation results, which adversely affects the subsequent target recognition. In order to solve the problem of ambiguity and uncertainty of image pixel attribution, some scholars have introduced fuzzy mathematical methods. The fuzzy C-mean clustering [8] method has obvious advantages in the field of image segmentation, such as fast convergence and simple operation, and has received wide attention, but it is still sensitive to the influence of noise, and the segmentation accuracy still needs further improvement. The fuzzy entropy principle that our work is based on is described below.

2.1. Fuzzy entropy principle based on probability partition

In the literature [19], fuzzy entropy has been proposed, dependent on the parameters for how the membership performs. In our work, the three-level thresholding parameters represented a

random combination and to develop effective fitness functions that will result in high-quality image segmentation.

Let D = {(i, j): i = 0, 1, …, R-1; j = 0, 1, …, C-1}, H = {0, 1, …, I-1}, where R, C, I∈N+, the gray levels I of the size of the paper's image is 256. The gray breast mammography image defines a matrix I = {D→H}. Let I (x, y) represent the gray level value for the pixel (x, y) in the image:

$$D_k = \left\{ I(x,y) = k \middle| \forall (x,y) \in D, I(x,y) \in H \right\} \tag{1}$$

where k = 0, 1, …, I-1, let n_k denotes the number of pixels in D_k. Then, the proportion of the gray level value k is defined as follows:

$$h_k = \frac{n_k}{R * C} \tag{2}$$

where $0 \le h_k \le 1$,Thus, the histogram of the image h = {h0, h1, …, hl-1} and h = 1. The following conclusions can be easily formed:

$$D_k = \left\{ \bigcup_{k=0}^{l-1} D_k = D \middle| D_{k_1} \cap D_{K_2} = \Phi, k_1 \ne k_2 \right\} \tag{3}$$

$\Pi = \{D_0, D_1, \ldots, D_{l-1}\}$ is a probability partition of D with a probabilistic distribution is $p_k = P(D_k) = h_k$. The two thresholds can form the three-level segmentation image, Name the two segmentation thresholds t_1 and t_2. Then they divide the image into three gray level, represent bright levels, medium levels and dark levels. A fuzzy set is an extension of a classical set in which elements can partially belong to a set, such as $w = \{x, \mu_w(x)\}$, where $0 < \mu_w(x) < 1$ is denoted the membership function. Let three gray leve D_k take the three sets of two thresholds separately: $D_k < t_1, t_1 < D_k < t_2$, and $D_k > t_2$. A constraint is $p_{d|k} + p_{m|k} + p_{b|k} = 1$ (k = 0, 1, …, 255). Then we can get that:

$$p_d = \sum_{k=0}^{255} P\left(D_{d|k}\right) = \sum_{k=0}^{255} p_k * \mu_d(k) \tag{4}$$

$$p_m = \sum_{k=0}^{255} P\left(D_{m|k}\right) = \sum_{k=0}^{255} p_k * \mu_m(k) \tag{5}$$

$$p_b = \sum_{k=0}^{255} P\left(D_{b|k}\right) = \sum_{k=0}^{255} p_k * \mu_b(k) \tag{6}$$

Definition 2.3. Let D_d, D_m and D_b be the dark, medium and bright value of fuzzy entropy, Then the total fuzzy entropy Ft is respectively denoted as following:

$$F_t = \sum_{k=0}^{255} \frac{p_k * \mu_d(k)}{p_d} * \ln\left(\frac{p_k * \mu_d(k)}{p_d}\right) + \sum_{k=0}^{255} \frac{p_k * \mu_d(k)}{p_d} * \ln\left(\frac{p_k * \mu_d(k)}{p_d}\right) + \sum_{k=0}^{255} \frac{p_k * \mu_d(k)}{p_d} * \ln\left(\frac{p_k * \mu_d(k)}{p_d}\right) \tag{7}$$

2.2. Differential evolution

Differential evolution is a population based on real number coding regarded as a global search strategy, originally introduced by Price and Storn [20]. In the evolution, the initially population enters the iteration process through variation, crossover and selection until the stopping condition is satisfied. Each individual in the population represents a candidate solution of the objective function f(x), which evaluates its quality by calculating the adaptive function and records the optimal individual.

The population is initialized as follows: the dimension of feasible solution space *B*, the population size *NP*, and x^G represents the *G* generation population. Each individual $x_{i,j}^G$ is made up of *B* dimensional parameters:

$$v_i^G = x_{r_1}^G + F \cdot \left(x_{r_2}^G - x_{r_3}^G\right), r_1, r_2, r_3 \in \{1,2,..., NP\} \tag{8}$$

where is $x_{i,j}^G$ randomly chosen within the range$[x^L, x^U]$, x^L and x^U represent the lower bound and upper bound.

At this stage, the parent population x_i^G produce variant individual v_i^G by mutation strategies, F [0,1]. The indices r_1, r_2, r_3 should be mutually exclusive and are generated randomly once every mutant vector within the range of [1, *NP*]. The commonly used mutation operator can be formulated as follows:

$$v_i^G = x_i^G + F_i \cdot \left(x_{r_2}^G - x_{r_3}^G\right) \tag{9}$$

Cross operation's main function is to generate the trail vector u_i from the target vector x_i and the mutated vector v_i. The crossover operation of the DE algorithm, which uses a binomial cross scheme, can be written as follows:

$$u_i^G = \begin{cases} v_i^G, rand_j \le CR \quad or \ j = j_{rand} \\ x_i^G, \qquad\qquad\qquad \text{overwise} \end{cases} \tag{10}$$

where j_{rand} is a random integer between 1 and B, representing the arbitrary dimension between the mutation vector and the target vector. The crossover control parameter is *CR*, and $rand_j$ is a uniformly distributed random number between 0 and 1. In addition, in order to improve the DE's search capabilities, Wang [21] suggested using an orthogonal crossover operation as opposed to the more

common binomial or exponential. A rotationally invariant crossover (like the one described by Wang et al. [22]) will more successfully follow the function landscape and will produce better trial vectors, according to Guo and Yang [23].

The survival of the fittest model is primarily used in the selection operation. The offspring are always superior to or equal to their parents. The population accepts the trail vector u_i if and only if its fitness value is greater than the fitness value of the target vector x_i. Otherwise, x_i is still in the following generation:

$$x_i^{G+1} = \begin{cases} u_i^G, if\ f\left(u_i^G\right) \le f\left(x_i^G\right) \\ x_i^G, \qquad \text{overwise} \end{cases} \tag{11}$$

where f(x) is the objective function.

3. Algorithm model

3.1. DE parameter Adaptation

DE/rand/1 is widely used in DE mutation strategy and developed for DE in the literature. However, [24] indicates that a set of candidate strategies have local mutation and global mutation perhaps has some benefits over DE/rand/1. Also, the authors of [25] proposed a multi population with three mutations. Gland segmentation is converted into a real solving problem. A fast and dependable convergence performance of greedy strategies is required for the problem. In this paper, a new mutation operator called DE/current-to-K-best is proposed. A mutation strategy DE/current-to-K-best/1 is Formulated as following manner:

$$\mathrm{v_i^G} = \mathrm{x_i^G} + \mathrm{F_i} \cdot \left(\mathrm{x_{best}^{G,K}} - \mathrm{x_i^G}\right) + \left(\mathrm{x_{r_1}^G} - \mathrm{x_{r_2}^G}\right) \tag{12}$$

where $\mathrm{x_{best}^{G,K}}$ is consistently selected as one of the top K solutions in the current K(0,1] solutions.

3.2. DE parameter Adaptation

The value of F is a fixed value and cannot be used to solve all global optimization functions in the conventional DE strategy. The scaling factor *F* mostly utilizes the Cauchy inverse cumulative distribution in our work. Let $F_{i,j}$ be the individual's crossover probability for each dimension. $F_{i,j}$ is written as follows:

$$F_{i,j} = Cauchy_{i,j}\left(Fm_j, 0.1\right) \tag{13}$$

where *Fm* is the scaling factor for the current individual and the positioning parameter of the Cauchy inverse cumulative distribution. The initial *Fm* is 0.5, and the scale parameter 0.1. Denote S_{Fj} as the successful crossover parental scaling factor, Fm_j is written as follows:

$$\mathrm{F}m_j = \left(1-c\right) \cdot Fm_j + c \cdot mean_F\left(S_{F,j}\right) \tag{14}$$

where c is a positive constant ranging from 0 to 1 and $mean_F(.)$ is the Lehmer mean operation is as follow:

$$mean_F\left(S_{F,j}\right)=\frac{\sum_D F^2}{\sum_D F} \tag{15}$$

Cross probabilities CR determine the likelihood of the target individual to inherit a gene from the variant individual v_i^G. CR uses a normal distribution, and $CR_{i,j}$ represents the crossing probability of each individual dimension in the proposed algorithm. Denote $S_{CR,j}$ as the successful crossover parental crossover probability, $CR_{i,j}$ is written as follows:

$$CR_{i,j}=randn_{i,j}\left(CRm_j,0.1\right) \tag{16}$$

where *CRm* is the average of the individual crossover probability, the initial value 0.5, and the standard deviation 0.1, *CRm* is expressed as follows:

$$CRm_j=\left(1-c\right)\cdot CRm_j+c\cdot mean_{CR}\left(S_{CR,j}\right) \tag{17}$$

where $mean_{CR}(.)$ is usual arithmetic mean operation.

3.3. Fitness function

The three gray levels have six parameters for gland segmentation, $x_i=\{x_{i,1},x_{i,2},x_{i,3},x_{i,4},x_{i,5},x_{i,6}\}$; After decoding x_i to segment breast gland, the value of the fitness function $f(x_i)$. The $f(x_i)$ is calculated by evaluating F_t according to Eq (7). As DEalgorithm is essentially designed to solve positive minimization problems, by constructing our fitness function as F_t:The three membership functions are shown in Figure 2, and give the membership functions detail information.

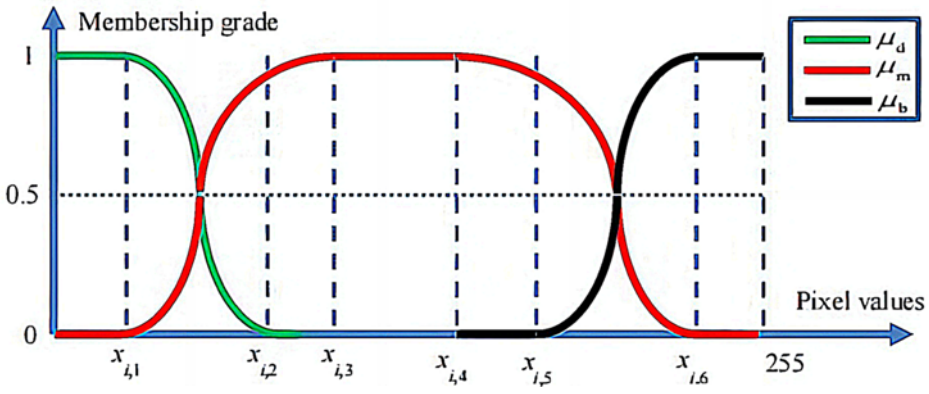

Figure 2. Plots of fuzzy membership functions with their six support points.

where $x_i=\{x_{i,1},x_{i,2},x_{i,3},x_{i,4},x_{i,5},x_{i,6}\}$ satisfy the following condition, $0<x_{i,1}<x_{i,2}<x_{i,3}<x_{i,4}<x_{i,5}<x_{i,6}<255$ The optimal parameter x_i that the minimum value of the total fuzzyentropy and the minimum value of fitness function. Then the most appropriate combination of thresholds, by

which the image is segmented into three classes, can be computed as following:

$$\mu_d(t_1) = \mu_m(t_1) = 0.5 \tag{18}$$

Based on membership functions detail information in Figure 2, the optimal thresholds $\{t_1,\ t_2\}$can be given below:

1) If $(x_{i,1} + x_{i,3})/2 \le x_{i,2} \le x_{i,3}$, then $t_1 = x_{i,1} + \sqrt{(x_{i,3} - x_{i,1}) * (x_{i,2} - x_{i,1})/2}$;

2) If $x_{i,1} \le x_{i,2} < (x_{i,1} + x_{i,3})/2$, then $t_1 = x_{i,3} - \sqrt{(x_{i,3} - x_{i,1}) * (x_{i,3} - x_{i,2})/2}$;

3) If $(x_{i,4} + x_{i,6})/2 \le x_{i,5} \le x_{i,6}$, then $t_2 = x_{i,4} + \sqrt{(x_{i,6} - x_{i,4}) * (x_{i,5} - x_{i,4})/2}$;

4) If $x_{i,4} \le x_{i,5} < (x_{i,4} + x_{i,6})/2$, then $t_2 = x_{i,6} - \sqrt{(x_{i,6} - x_{i,4}) * (x_{i,6} - x_{i,5})/2}$;

3.4. Improved differential evolutionary optimization fuzzy entropy

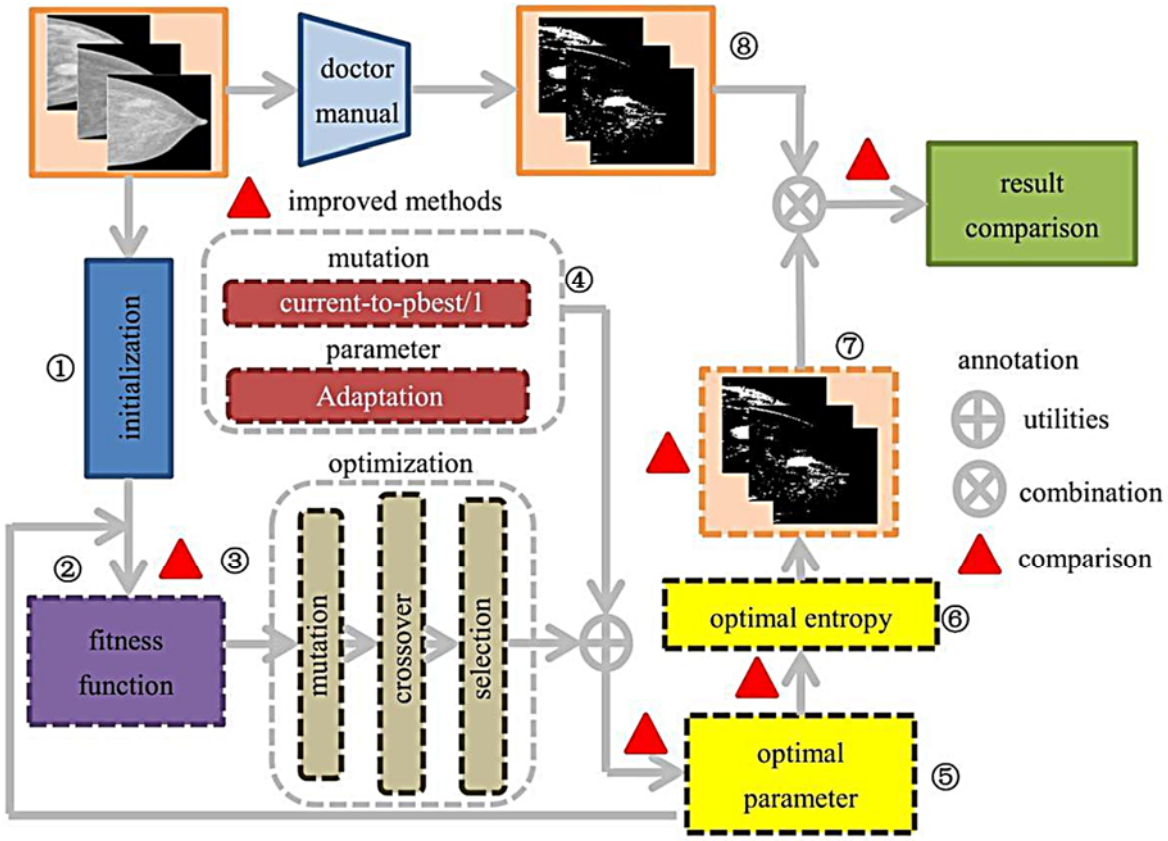

Figure 3. The framework of IDE algorithm optimizes the fuzzy entropy for the segmentation gland.

Figure 3 shows that the framework of IDEFE how to segment breast gland in mammography image. First, module ① initialize parameters as initial evolutionary individuals for calculate the fitness in ②; Then, in the optimization stage, the IDE combines ③ the ④ and to optimal parameter in module ⑤; Until not satisfy the condition; Finally, the segmentation result ⑦ is determined by the module ⑥, which can be compared with doctor manual result ⑧. According to the fuzzy entropy

criterion, the breast image is divided into black (air), gray (soft tissue) and white (breast gland). A large fuzzy entropy indicates that the set is fuzzy. However, gland segmentation requires an overall determined fuzzy set and small uncertain edges. Thus, the fitness function requires a minimum value, in order to segment significant gland area.

As the framework of the Figure 3, a new segmentation algorithm, called IDEFE, is proposed. The IDEFE algorithm is described in Algorithm in detail. As discussed in the abstract, the optimization fuzzy entropy gland segmentation with edge blurring and premature convergence is a complex problem. The optimal solution cannot be obtained quickly by the global search method, resulting in unclear edge segmentation. In our work, on the one hand, DE/current-to-K-best/1 is semi-local strategy, which cannot blindly search the global optimal solution. On the other hand, the parameter adaptation automatically updates the control parameters to appropriate values and avoids a user's prior knowledge of the relationship between the parameter settings and the characteristics of optimization problems. It clearly shows that the improved points can provide global optimum solution and fast convergence. As such, a new optimization algorithm, called IDE, is proposed. The DE/current-to-K-best/1 operator and adaptation parameter are denoted by $\bullet$, where fitness value according to Eq (7); the scale factor *Fm* according to Eqs (13)–(15); the crossover factor *CRm* according to Eqs (16) and (17); the mutation vector v_i according to Eq (12); the trail vector u_i according to Eq (10); the optimal solution x_i for the next generation according to Eq (11), the optimal thresholds according to Eq (18); The details of this algorithm arespecified as follows.

Algorithm: IDEFE

Initialization: Set *fes* = 1; Initialize all parameters for the DE algorithm;

- three gray levels have six parameters $x_i = \{x_i^1, x_i^2, x_i^3, x_i^4, x_i^5, x_i^6\}$;
- Calculate fitness value;

Results: The optimal fitness value fbest and optimal thresholds $\{t_1, t_2\}$;

Repeat

- Calculate fitness value;

if *fes* > 1

- update the scale factor *Fm*;
- update the crossover factor *CRm*;
- Calculate the mutation vector v_i;
- Calculate the trail vector u_i;
- Select the optimal solution x_i for the next generation;
- Reserved the optimal parameter $\{SF_J, SCR_J\}$;
- Determine the optimal thresholds.
- Reserved the fitness value fbest and optimal thresholds$\{t_1, t_2\}$, *fes* = *fes* +1;

Until the evolution not satisfy the iteration condition;

4. Experiment results and discussion

4.1. Breast mammography images

The breast mammography image and corresponding label are acquired from Quanzhou First Hospital, Fujian, China [26]. The BIRADS classifies the breast into four categories, proposed by the

American Radiation Association [27]. The fat mammary glands accounts for less than 25%, the few accounts for 25–50%, the multi-type accounts for 51–75%, and the extremely accounts for more than 75%. The corresponding type of breast mammogram images have corresponding serial numbers, such as 133953_RCC_fat, 310679_LCC_few. Where the leading number represents the image number, RCC is denoted as right craniocaudal, and LCC is left craniocaudal. As in Figure 7(a) there are right breast images and left breast images. Since the serial number is too long, renamed #1~#18, respectively. As mentioned above, Figure 4 experimental data set and label distribution show 4 cases of fat glands, 4 cases of few glands, 6 cases of multiple glands and 4 cases of extremely glands.

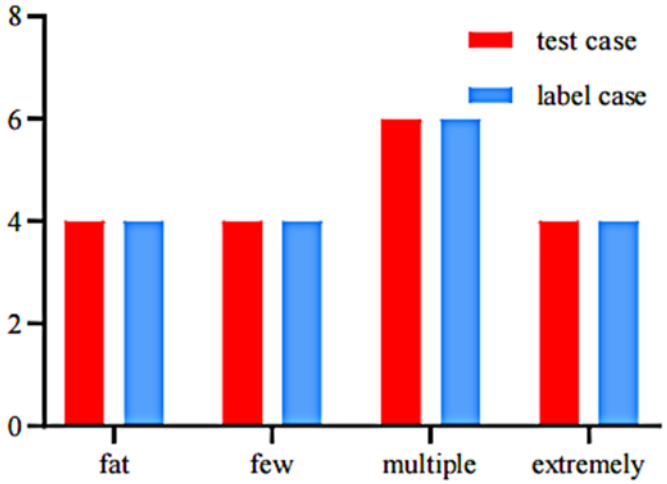

Figure 4. Experimental data set and label distribution.

4.2. Image qualitative evaluation

Based on the computer field, the image quality assessment of Structural Similarity is proposed by Wang and Bovik [19]. The SSIM measurement system's similarity measurement can be divided into three comparison modules: brightness, contrast, and structure. The single comparable measurement function ssim(x, y) is constructed by combining the three comparison modules:

$$ssim(x,y)=\frac{(2\mu_x\mu_y+C_1)(2\sigma_x\sigma_y+C_2)}{(\mu_x^2+\mu_y^2+C_1)(\sigma_x^2+\sigma_y^2+C_2)} \tag{19}$$

where μ_x represents the brightness comparison function of the label image. Thus, the result image is μ_y. C_1 and C_2 are fixed numbers. Then, the MSSIM index is used as the estimated quality evaluation of the entire image, which can be expressed as:

$$mssim(x,y)=\frac{1}{MN}\sum_{1}^{M}\sum_{1}^{N}ssim(x_a,y_a) \tag{20}$$

where x_a and y_a are the locations of the local SSIM index in the map, and M and N are the number of local windows.

The doctor manually regarded as a comparison label, which can be used for comparing with the

result image. Then, Figure 5 shows the mssim of algorithms 100 times independent tested on 18 breast images. Form the Figure 5A1, each test result of IDEFE is more uniform than other algorithms.

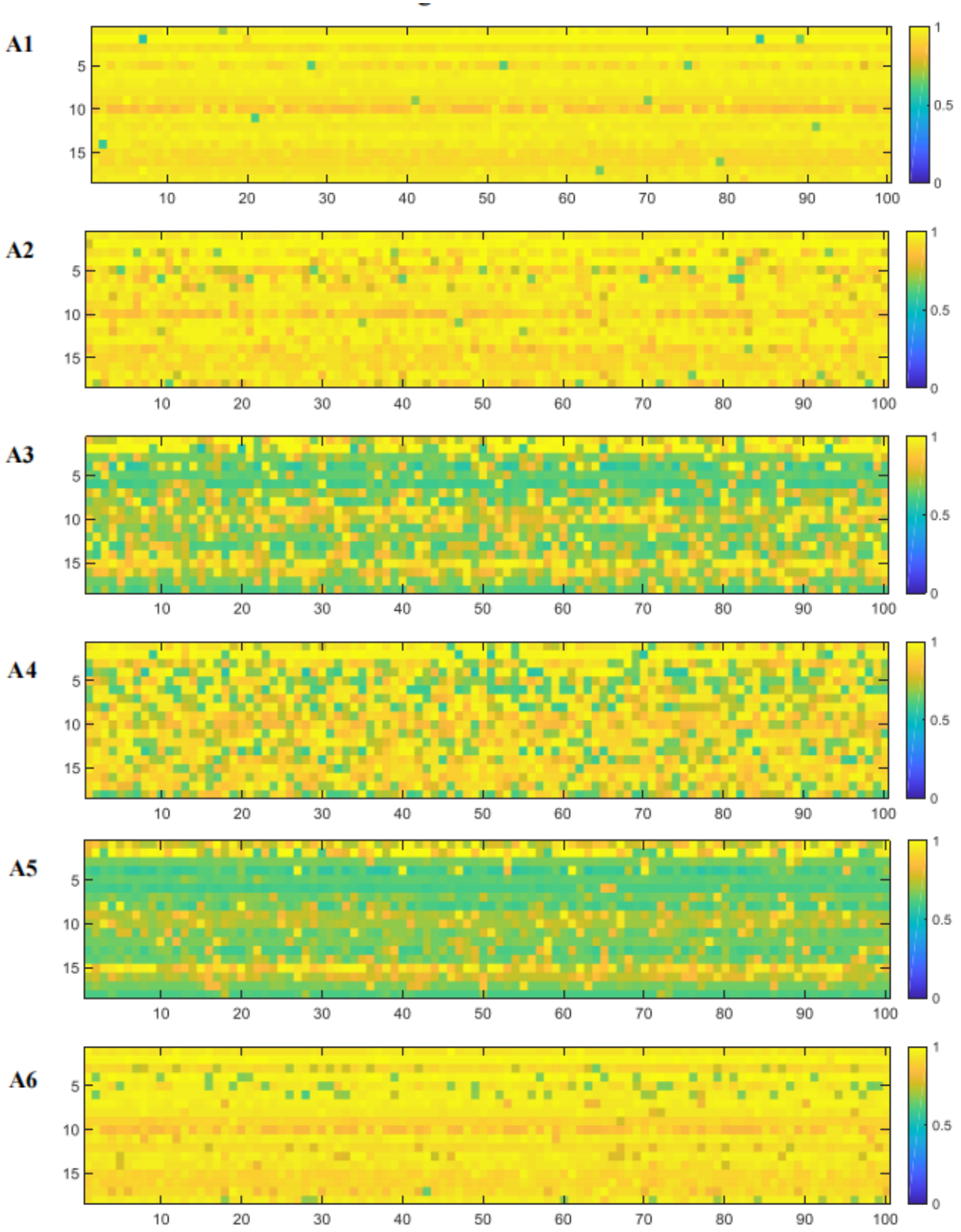

Figure 5. The 100 times mssim of IDEFE, DEFE, FireflyFE, BatFE, ABCFE, and PSOFE independent tested on18 breast images. A1: IDEFE, A2: DEFE, A3: FireflyFE, A4: BatFE, A5: ABCFE, A6: PSOFE.

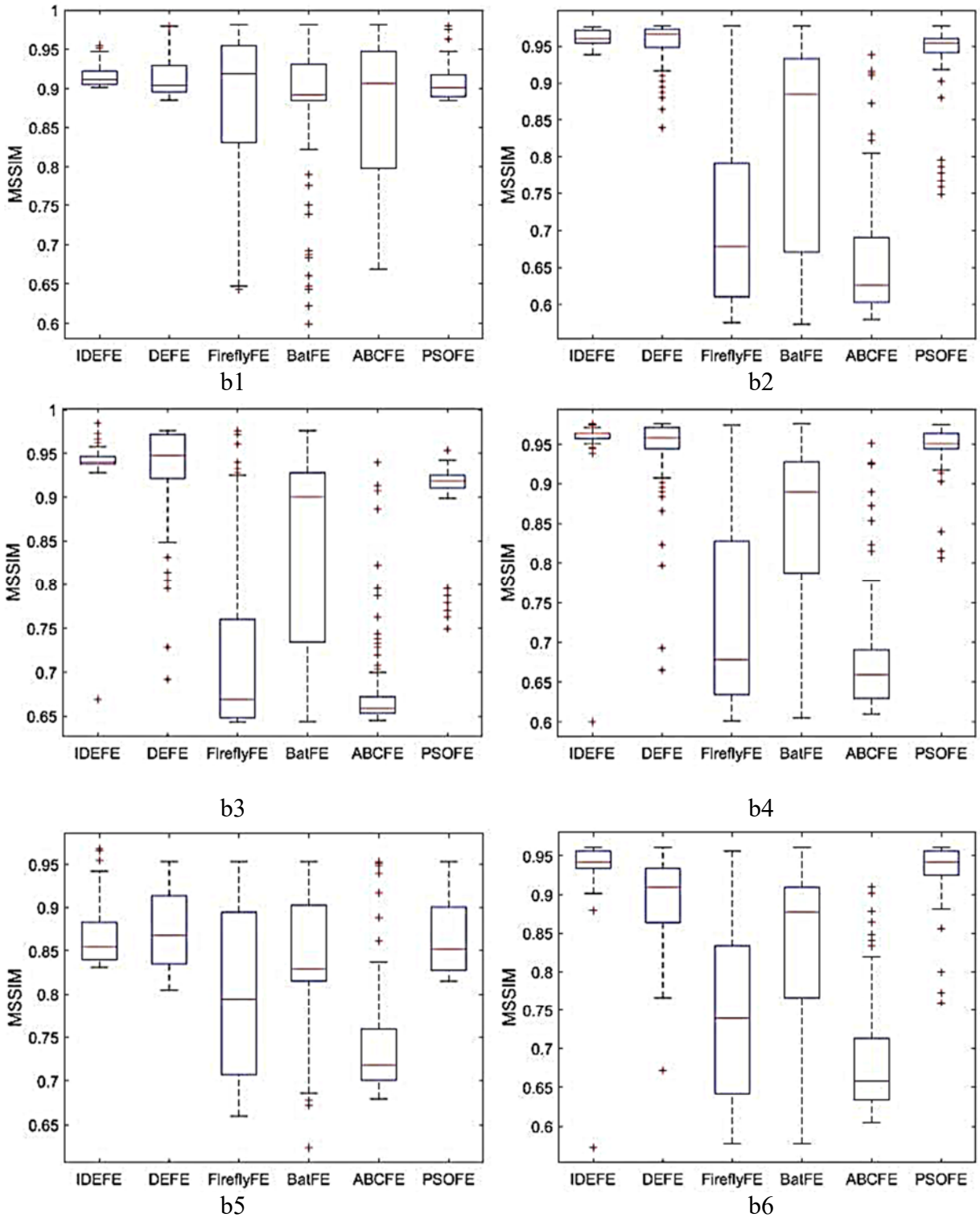

Figure 6. Boxplot the MSSIM of IDEFE, DEFE, FireflyFE, BatFE, ABCFE, and PSOFE with 100 times independent tested on 6 breast images.

In order to get the distribution of MSSIM in detail, Figure 6 shows the MSSIM of differential algorithms 100 times independent tested on 6 breast images by the boxplot. From the (b4) in Figure 5, the median MSSIM value of IDEFE is not better than DEFE. Whereas, DEFE has outliers 12, 7 and 7 in the (b4) which represent poor solution robustness. The MSSIM result of FireflyFE, BatFE and

ABCFE fluctuate over a range of 0.05 in the (b1), (b4), the MSSIM result of DEFE and PSOFE vary widely in the (b3), (b6). Noted that the distance of between the maximum MSSIM and the minimum in Figure 6, the overall robustness performance of IDEFE is superior to all comparative algorithms. From the mean MSSIM and the boxplot, evidences have shown that mutation strategy may be efficient in searching landscapes of segmentation gland problems.

4.3. Results and discussion

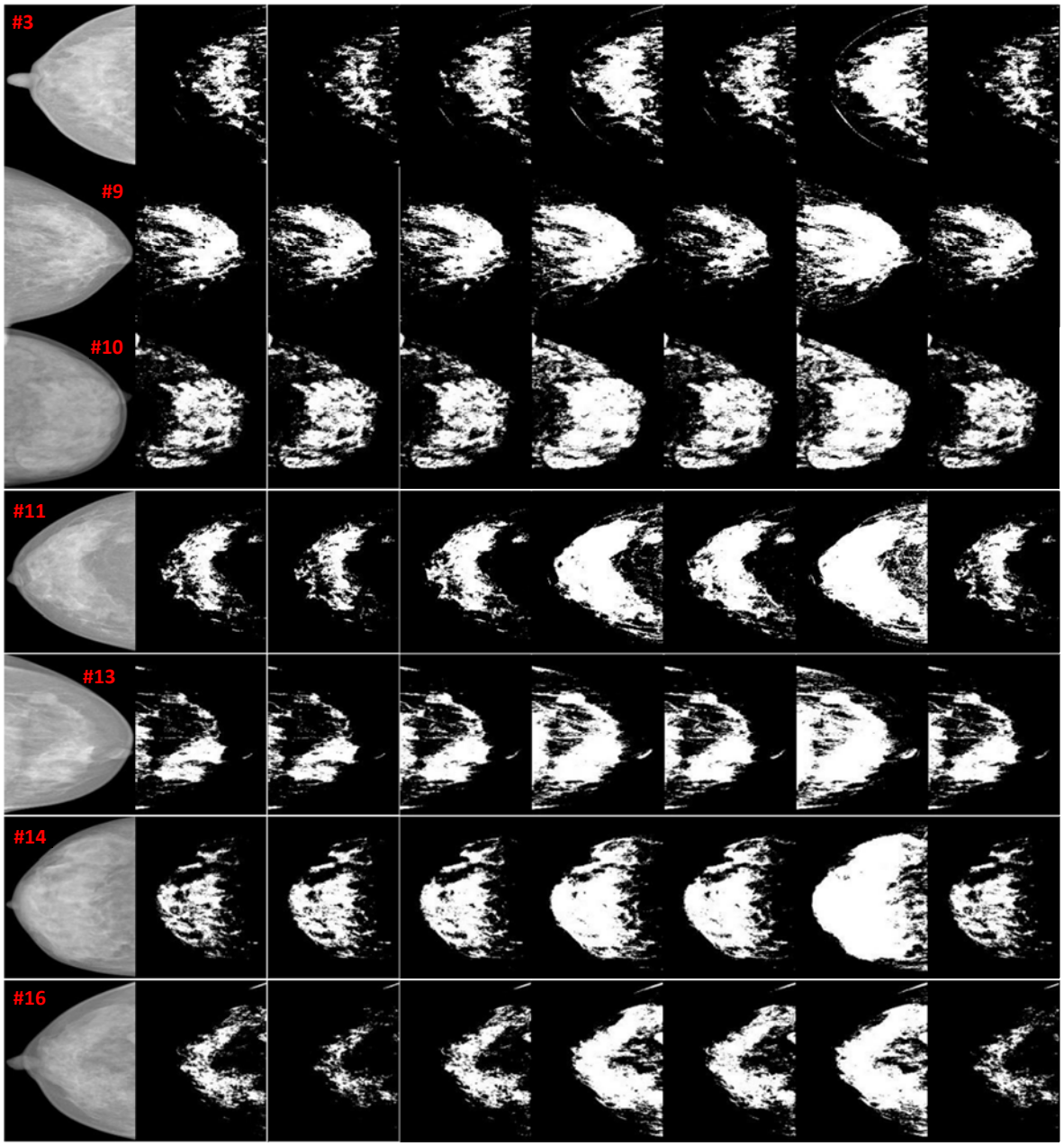

Figure 7. The median MSSIM segmentation result of IDEFE, DEFE, FireflyFE, BatFE, ABCFE, and PSOFE with 100 times independent tested on #3, #9, #11, #13 and #16 multiple type, #10 and #14 extremely dense. (a) raw data, (b) ground truth, (c) IDEFE, (d) DEFE, (e) FireflyFE, (f) BatFE, (g) ABCFE, (h) PSOFE.

Figure 7 #3, #9, #11, #13 and #16 show the median MSSIM results of the segmentation result of few gland images with 100 times tested by different algorithms. The ground truth of which are the results of manual segmentation by experts from the Fujian Provincial Medical Association Breast Disease Branch and verified with the assistance of experts from Quanzhou First Hospital. Although DEFE outperforms MPEDE on image #9 and #16, MPEDE is capable of finding the optimal solutions for these three images #3, #11 and #13. Since the gland brightness and background of #9 and #16 are not much different, the excessive solution of the fuzzy entropy is to divide part of the dark gland into the background area. From the #10 and #14 in Figure 7, DEFE, FireflyFE, BatFE, ABCFE, and PSOFE are not able to produce a better segmentation result than IDEFE on any of the extremely dense images.

Additionally, the solution-searching process is guided by the mutation strategy DE/current-to-K-best/1, which may result in a situation where the solution is a global optimum of the criterion. The adaptation parameters inherit the parameters of the better parent solution, which can ensure the robustness of the proposed algorithm. This problem can be solved in the future by using a multi-objective optimization approach to capitalize on the strengths of other criteria. At present, there are some image processing algorithms that combine fuzzy theory and deep learning, but they are rarely used in the field of image segmentation, and these algorithms still have many problems to be studied and solved. For this reason, in our future work, we will study in depth the description of image data uncertainty during image segmentation, the improvement of fuzzy algorithms, and the combination of CNN in deep learning with fuzzy theory related algorithms. That is, the concept of fuzzy learning is introduced in deep learning to overcome the shortcomings of fixed representation and achieve the improvement of segmentation accuracy. Convolutional units can be used to extract discriminative features at different scales, thus providing comprehensive information for pixel-level image segmentation.

5. Conclusions

For the segmentation of breast gland mammography images, a new double threshold method called IDEFE is presented in this paper. It combines the benefits of an improved DE algorithm with fuzzy entropy segmentation. Superior segmentation outcomes have been achieved in part by partially overcoming the two main limitations of optimization fuzzy entropy algorithms, which are the susceptibility to irregular edges and the premature convergence. The IDEFE algorithm and five comparison algorithms have been tested on 18 real breast gland mammography images. The experimental results demonstrate that the proposed algorithm outperforms five existing state-of-the-art techniques described in the literature. Especially, on the one hand, the proposed algorithm demonstrates greater compactness and has fewer artifacts than others on the computer image segmentation indicator; on the other hand, the medical segmentation indicator also demonstrates the superiority of the IDEFE algorithm in comparison to the competitors.

Acknowledgments

The authors warmly recognize the kind collaboration of the First Hospital of Quanzhou during the data picture gathering process. This work was supported by the Grants from National Natural Science Foundation of Fujian (2021J011394, 2021J011404), in part by the Quanzhou scientific and technological planning projects (2021C037R).

Conflict of interest

The authors declare there is no conflict of interest.

References

1. R. L. Siegel, K. D. Miller, H. E. Fuchs, A. Jemal, Cancer statistics, 2022, *Ca A Cancer J. Clin.*, **72** (2022), 7–33. https://doi.org/10.3322/caac.21708
2. S. Lei, R. Zheng, S. Zhang, S. Wang, R. Chen, K. Sun, et al., Global patterns of breast cancer incidence and mortality: A population-based cancer registry data analysis from 2000 to 2020, *Cancer Commun.*, **41** (2021), 1183–1194. https://doi.org/10.1002/cac2.12207
3. W. Cai, B. Zhai, Y. Liu, R. Liu, X. Ning, Quadratic polynomial guided fuzzy C-means and dual attention mechanism for medical image segmentation, *Displays*, **70** (2021), 102106. https://doi.org/10.1016/j.displa.2021.102106
4. H. Yazid, S. N. Basah, S. A. Rahim, M. J. A. Safar, K. S. Basaruddin, Performance analysis of entropy thresholding for successful image segmentation, *Multimed. Tools Appl.*, **81** (2022), 6433–6450. https://doi.org/10.1007/s11042-021-11813-z
5. A. Ciaramella, D. Nardone, A. Staiano, Data integration by fuzzy similarity-based hierarchical clustering, *BMC Bioinf.*, **21** (2020), 350–350. https://doi.org/10.1186/s12859-020-03567-6
6. N. Petrick, H. P. Chan, B. Sahiner, M. A. Helvie, Combined adaptive enhancement and region growing segmentation of breast masses on digitized mammograms, *Med. Phys.*, **26** (1999), 1642–1654. https://doi.org/10.1118/1.598658
7. N. Otsu, A threshold selection method from gray-level histograms, *IEEE Trans. Syst. Man Cybern.*, **9** (1979), 62–66. https://doi.org/10.1109/TSMC.1979.4310076
8. D. Tran, M. Wagner, Fuzzy entropy clustering, in *Ninth IEEE International Conference on Fuzzy Systems*, FUZZ-IEEE, **1** (2000), 152–157. https://doi.org/10.1109/FUZZY.2000.838650
9. A. Yezzi, S. Kichenassamy, A. Kumar, P. Olver, A. Tannenbaum, A geometric snake model for segmentation of medical imagery, *IEEE Trans. Med. Imaging*, **16** (1997), 199–209. https://doi.org/10.1109/42.563665
10. M. Versaci, F. C. Morabito, Image edge detection: A new approach based on fuzzy entropy and fuzzy divergence, *Int. J. Fuzzy Syst.*, **23** (2021), 918–936. https://doi.org/10.1007/s40815-020-01030-5
11. N. Mu, H. Wang, Y. Zhang, J. Jiang, J. Tang, Progressive global perception and local polishing network for lung infection segmentation of COVID-19 CT images, *Pattern Recognit.*, **120** (2021), 108168. https://doi.org/10.1016/j.patcog.2021.108168
12. J. He, Q. Zhu, K. Zhang, P. Yu, J. Tang, An evolvable adversarial network with gradient penalty for COVID-19 infection segmentation, *Appl. Soft Comput.*, **113** (2021), 107947. https://doi.org/10.1016/j.asoc.2021.107947
13. M. H. Horng, Multilevel thresholding selection based on the artificial bee colony algorithm for image segmentation, *Expert Syst. Appl.*, **38** (2011), 13785–13791. https://doi.org/10.1016/j.eswa.2011.04.180
14. Z. W. Ye, M. W. Wang, W. Liu, S. B. Chen, Fuzzy entropy based optimal thresholding using bat algorithm, *Appl. Soft Comput.*, **31** (2015), 381–395. https://doi.org/10.1016/j.asoc.2015.02.012

15. M. S. R. Naidu, P. R. Kumar, Multilevel image thresholding for image segmentation by optimizing fuzzy entropy using Firefly algorithm, *Int. J. Eng. Technol.*, **9** (2017), 472–488. https://doi.org/10.21817/ijet/2017/v9i2/170902013
16. S. Dhar, M. K. Kundu, A novel method for image thresholding using interval type-2 fuzzy sets and bat algorithm, *Appl. Soft Comput.*, **63** (2018), 154–166. https://doi.org/10.1016/j.asoc.2017.11.032
17. C. W. Lin, T. P. Hong, A survey of fuzzy web mining, *WIRE Data Min. Knowl. Discovery*, **3** (2013), 190–199. https://doi.org/10.1002/widm.1091
18. C. W. Lin, T. P. Hong, W. H. Lu, Linguistic data mining with fuzzy FP-trees, *Expert Syst. Appl.*, **37** (2010), 4560–4567. https://doi.org/10.1016/j.eswa.2009.12.052
19. J. Li, W. Tang, J. Wang, X. Zhang, Multilevel thresholding selection based on variational mode decomposition for image segmentation, *Signal Process.*, **147** (2018), S0165168418300306. https://doi.org/10.1016/j.sigpro.2018.01.022
20. R. Storn, K. Price, Differential evolution—A simple and efficient heuristic for global optimization over continuous spaces, *J. Global Optim.*, **11** (1997), 341–359. https://doi.org/10.1023/A:1008202821328
21. Y. Wang, Z. Cai, Q. Zhang, Enhancing the search ability of differential evolution through orthogonal crossover, *Inf. Sci.*, **185** (2012), 153–177. https://doi.org/10.1016/j.ins.2011.09.001
22. S. M. Guo, C. C. Yang, Enhancing differential evolution utilizing eigenvector-based crossover operator, *IEEE Trans. Evol. Comput.*, **19** (2015), 31–49. https://doi.org/10.1109/TEVC.2014.2375933
23. Z. J. Wang, Z. H. Zhan, Y. Lin, W. J. Yu, H. Wang, S. Kwong, et al., Automatic niching differential evolution with contour prediction approach for multimodal optimization problems, *IEEE Trans. Evol. Comput.*, **24** (2019), 114–128. https://doi.org/10.1109/TEVC.2019.2910721
24. Y. Wang, Z. Cai, Q. Zhang, Differential evolution with composite trial vector generation strategies and control parameters, *IEEE Trans. Evol. Comput.*, **15** (2011), 55–66. https://doi.org/10.1109/TEVC.2010.2087271
25. G. Wu, R. Mallipeddi, P. N. Suganthan, R. Wang, H. Chen, Differential evolution with multipopulation based ensemble of mutation strategies, *Inf. Sci.*, **329** (2015), 329–345. https://doi.org/10.1016/j.ins.2015.09.009
26. Y. Fan, P. Liu, J. Tang, Y. Luo, Y. Du, Fuzzy entropy based on differential evolution for breast gland segmentation, *Australas Phys. Eng. Sci. Med.*, **41** (2018), 1101–1114. https://doi.org/10.1007/s13246-018-0672-5
27. S. G. Orel, N. Kay, C. Reynolds, D. C. Sullivan, BI-RADS categorization as a predictor of malignancy, *Radiology*, **211** (1999), 845–850. https://doi.org/10.1148/radiology.211.3.r99jn31845

AIMS Press